Enhancing Power Transformer Reliability: High-Frequency Modeling, Transient Interactions, and Overvoltage Protection Scheme

Nasirpour, Farzad; Behdani, Behzad; Heidary, Amir; Ghaffarian Niasar, Mohamad; Ghassemi, Forooz ; van Riet, Maarten; Wilkinson, Mark; van der Meijden, M.A.M.M.; Popov, Marjan; More Authors

Publication date
2024

Document Version
Final published version

Published in
Cigre 2024 Proceedings

2024 Paris Session

10531
C4 POWER SYSTEM TECHNICAL PERFORMANCE
PS3 - Insulation Co-Ordination and Lightning Interference Analysis: Challenges, Opportunities and Advances

Enhancing Power Transformer Reliability: High-Frequency Modeling, Transient Interactions, and Overvoltage Protection Scheme

Farzad NASIRPOUR[1], Behzad BEHDANI[1], Amir HEIDARY[1], Mohamad GHAFFARIAN NIASAR[1], Forooz GHASSEMI[2], Kostas VELITSIKAKIS[3], Maarten van RIET[4], Mark WILKINSON[5], Mart van der MEIJDEN[3], Sjoerd NAUTA[4], Imre TANNEMAAT[3], Jos VEENS[5], and Marjan POPOV*[1]

1. **Delft University of Technology, Faculty of EEMCS, Delft, the Netherlands**
2. **National Grid Electricity Transmission plc, U.K.**
3. **TenneT TSO B.V., the Netherlands**
4. **Alliander N.V., the Netherlands**
5. **Royal SMIT Transformers B.V., the Netherlands**

E-Mail: f.nasirpour@tudelft.nl, b.behdani-1@tudelft.nl, a.heidary@tudelft.nl, m.ghaffarianniasar@tudelft.nl, fznghassemi@gmail.com, kostas.velitsikakis@tennet.eu, maarten.van.riet@qirion.nl, mark.wilkinson@sgbsmit.group, mart.vander.meijden@tennet.eu, sjoerd.nauta@alliander.com, imre.tannemaat@tennet.eu, jos.veens@sgb-smit.group, m.popov@tudelft.nl*.

SUMMARY

The evolution of electrical power systems demands an increasing reliance on unpredictable renewable energy resources (RES). However, integrating these resources poses challenges, as their intermittent nature introduces transient events that can significantly impact power transformers. These transient phenomena may initiate energy oscillations in the form of weakly-damped resonances between system elements, i.e., transmission lines and cables, transformers, and the grounding system. Such conditions may impose stresses beyond the tolerance of insulating materials, leading to fast lifetime degradation and, eventually, the failure of critical components in the network, such as the costly power transformers. The impedance of the grounding system can limit the dissipation of surges, hence, causing severe overvoltages upon transient phenomena. By employing detailed transient models of crucial system components, this research puts forward a comprehensive analytical study of the transient interactions. In this regard, an analytical high-frequency transformer winding model based on lumped elements, and wideband frequency-dependent models for cables and the grounding system derived by applying electromagnetic theory are presented. These models, integrated into electromagnetic transient software, enable the identification of vulnerabilities and examination of case studies involving lightning strikes and switching events. Furthermore, the details of a novel protection method applied to safeguard the transformer are discussed in this paper. The presented protection method consists of a ring toroid core and a resistive suppressor on the secondary side of the core. This protection component is connected in series with the transformer to decrease the harmonic content and magnitude of the transient signals. The design procedure of the series protection device against voltage transient signals is presented and elaborated.

KEYWORDS

Protection, System Interaction, Transients, Transformer Modeling.

INTRODUCTION

The paradigm shift in electrical power systems, driven by the urgent need to combat climate change, has steered the focus toward harnessing renewable energy resources (RES). While promising, integrating RES introduces complexities, particularly concerning the reliable operation of power transformers. The unpredictable nature of these resources leads to frequent system changes due to many switching operations. Moreover, along with the expansion and interconnection of electrical power systems, they have become more susceptible to external disturbances from phenomena such as lightning strikes. These events are associated with the redistribution of electrical and magnetic energies between the components of the system, which take place accompanied by the excitation of the system's natural frequencies [1]. The resultant transient events can induce overvoltages with nonlinear distributions in transformer windings. Hence, the voltage may exceed the insulation withstand of a single or multiple winding coil(s), potentially compromising the transformer integrity and, consequently, the overall system reliability.

A significant contribution by CIGRE WG A2/C4.39 [1] focuses on this critical area, aiming to clarify the reasons behind transformer dielectric failures attributed to transient overvoltages. Their findings challenge the adequacy of existing factory-proof tests in standards, suggesting these tests might not comprehensively cover diverse transient events. Standard lightning impulse wave shapes may not reflect service conditions involving various scenarios such as reactor switching, HVDC converters, capacitor banks, GIS switching, and transformer energization via feeder cables. Additionally, the grounding system behaves differently across frequencies in real-world conditions compared to controlled lab settings [2]. Moreover, authors in [1] highlighted how resonance frequencies impact transformers, illustrating that specific network setups could induce oscillatory voltage waves at transformer terminals that coincide with their natural frequencies. This resonant voltage buildup can compromise insulation withstand capabilities, even at levels lower than their basic insulation level.

This inadequacy in addressing transient phenomena has led to reported failures [1]. For instance, in the United States [1], a single-phase fault caused flashovers in auto-transformers approximately 145 miles from the fault location. In Mexico, shell-form 230 kV generator step-up transformers experienced failures due to insufficient protection from lightning arresters and resonance excitation by lightning impulses [3]. In the United Kingdom [1], dielectric faults were encountered due to remote energization, causing internal over-voltages and leading to failures in power transformers. Failures in Brazil [1] also raised concerns about abnormal disconnector switching near equipment, causing unexplained dielectric failures in autotransformers. In Japan [1], lightning damaged distribution transformers multiple times due to internal resonance over-voltages. These failures highlight the necessity for deeper investigation into transformer-system interactions during transient events, emphasizing the need to consider both peak overvoltages and the frequency content of the transient.

By applying suitable transformer models, the interaction between network components and transformers can be studied. The effect of cable–transformer interactions on the currents and resonating voltages distributed along the transformer winding due to vacuum circuit breaker (VCB) prestriking transients were studied in [4]. An analytical study of cable–transformer interactions, focusing on the resonance overvoltages occurring on the secondary side of the transformer, was conducted in [5]. In [6], a detailed analysis of this phenomenon was carried out, focusing on the high-frequency interactions between cable systems and transformers and the topologies prone to such effects. This study demonstrated that a severe oscillating overvoltage condition may prevail when the resonance frequencies of the cable and transformer match one another. The impact of the external network on transformer internal voltages was studied in [7], where voltages on transformer terminals were mapped on critical points along the transformer winding with the help of a sectionized model. In [8], the resonances of cables connected to transformers were studied, highlighting the impact of cable terminal impedance.

Protecting transformers against these overvoltages is important and, as such, has been investigated in many scientific and industrial projects [9, 10]. Among various types of protection methods, series protection devices offer several advantages in protecting the transformers against transient signals. Their isolated design simplifies insulation requirements, contrasting with concerns faced by parallel protection devices for high-voltage systems [11-14].

The current research endeavors to elucidate the behavior of transformers during transient events and develop robust protection schemes. The paper begins by presenting an analytical high-frequency

transformer winding model. Subsequently, a comprehensive grounding system model employing full-wave electromagnetic theory is also presented. Understanding the system vulnerabilities regarding mutual interactions between components during transient events calls for a unified simulation platform, taking into account detailed models of transformers, transmission lines/cables, and the grounding system. In this regard, EMT-type software is employed as the simulation platform for vulnerability identification analyses. The paper culminates in presenting a detailed analysis of a series protection method specifically designed for transformers, leveraging toroid cores' magnetic properties simulated by finite element methods (FEMs), as a practical measure against fast transients.

RESEARCH METHODOLOGY

1. POWER TRANSFORMER MODEL

Transformer models are categorized into three main types: black-box, white-box, and grey-box models [15] . Among these, the white-box modeling approach is particularly well-suited for transient studies involving overvoltages inside the transformer, as it provides detailed information about internal behavior and interactions with other components. However, for other types of system transients, simpler transformer models are typically used. White-box modeling provides analytical representations of transformers based on their internal physical characteristics. To obtain these physics-based models, transformers can be represented in one of two ways: 1) through basic lumped circuit elements that simplify windings down to inductances, resistances, and capacitances, or 2) through distributed parameters that capture the transmission line aspects. Studies like [16] demonstrate that lumped modeling offers sufficient accuracy for fast transients; this approach is also adopted in this study.
Implementing lumped-element approach involves subdividing transformer windings into smaller sections or units. Fig. 1 illustrates this model with elements L_{hv}, L_{lv}, M_{ij}, M_{in}, and $M_{jn,}$ which represent the self-inductances of the high voltage (HV) and low voltage (LV) winding sections, the mutual impedance between them, and with other components, respectively. Additionally, R_{hv} and R_{lv} denote the conductor resistances for the HV and LV winding sections, while capacitances C_{hv}, C_{lv}, C_{hl}, C_{hg}, C_{lg} account for capacitances of HV and LV sections, between HV/LV-sections, and between sections and the transformer tank and core. The procedure of determining the values of these elements is further explained in [13, 17].

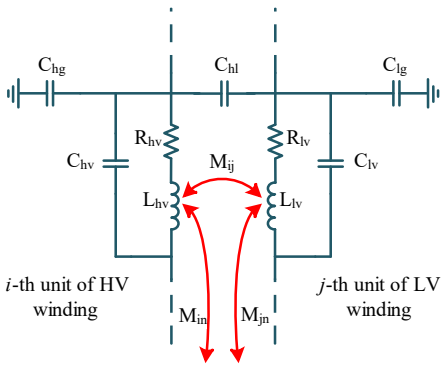

Fig. 1. An illustration of the transformer model.

Having all the elements, the model can be constructed. To validate the method's accuracy, the frequency response of an HV winding consisting of twenty-two disks, each with forty turns, is measured and compared with the model. This is shown in Fig. 2. In this model, each disk is considered as one section. The details of this winding are according to Table I.

2. GROUNDING SYSTEM MODEL

The electrical system grounding serves two purposes: ensuring personnel safety near high-voltage components and offering a return path for fault currents. The grounding system behaves resistively from power frequency up to several tens of kHz. However, for higher frequencies, the response to surge currents may be inductive or capacitive [18]. Accurately capturing grounding system response requires

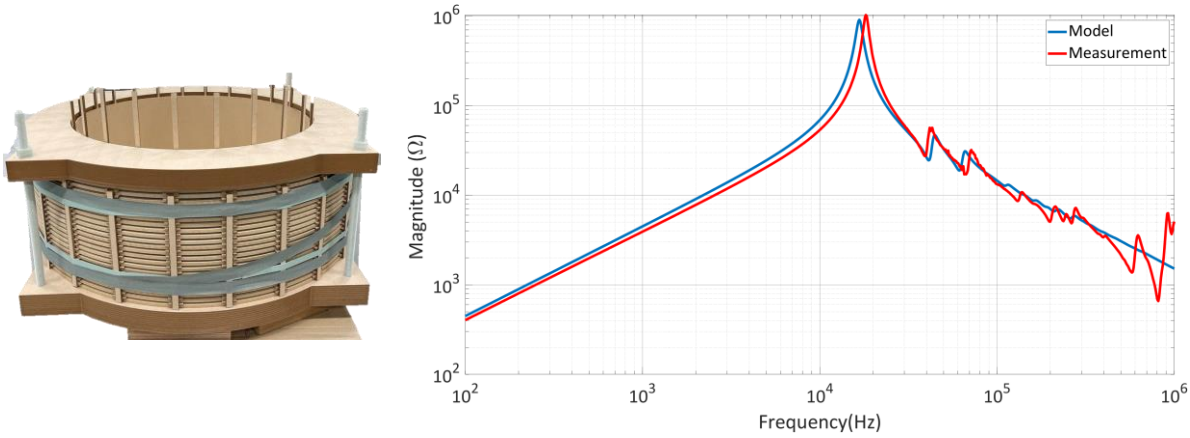

(a) (b)

Fig. 2. (a) High voltage winding of a transformer and (b) its terminal impedance.

TABLE I. DETAILS OF THE TEST WINDING.

Number of Disks	22
Number of turns per disk	40
Conductor dimensions	1.8 mm ×× 8 mm
Conductor insulated dimensions	3.11 mm ×× 9.31 mm
Radial build	125.5 mm
Inner diameter	750 mm
Outer diameter	1001 mm
Vertical distance between disks	4 mm
Number of disks with three turns of shields	4
Number of disks with two turns of shields	4
Number of disks with one turn of shields	4
Number of disks with no shields	10

solving Maxwell's equations for conductors, which is challenging given the complexity of interconnected bare conductors in contact with the soil medium. This study utilizes electromagnetic theory to derive the grounding system response by incorporating the grounding grid's geometrical data, soil characteristics, and connection points to the network [19]. In this way, the grounding system's response is computed by applying a rigorous electromagnetic field theory, providing a bus impedance matrix seen from the grounding terminals [20].

Fig. 3(a) demonstrates a substation grounding grid, as an 80 m × 40 m rectangular network with 5 m × 5 m square meshes. The grounding grid is formed of interconnected copper conductors with a radius of 5mm, buried in the 0.5m depth of soil with a resistivity of 100 Ωm. To incorporate the grounding system's response, the impedances seen from the grounding terminals are obtained across the desired frequency spectrum. Subsequently, the vector fitting algorithm [21-23] is applied to synthesize the frequency-dependent impedances of the grounding system to be implemented in EMT-type programs for further analysis of system transients [24]. The response of the simulated grounding system obtained from the specified point and its implementation in an EMT-based software is illustrated in Fig. 3(b).

3. TRANSMISSION LINE/CABLE MODEL

Solving traveling wave equations, with reference to Fig. 4, enables modeling the terminal currents and voltages of the line/cable as a two-port network [25]:

$$\begin{bmatrix} \mathbf{I}_k \\ \mathbf{I}_m \end{bmatrix} = \left\{ \left(\mathbf{U} - \mathbf{H}^2 \right)^{-1} \begin{bmatrix} \mathbf{H}^2 + \mathbf{U} & -2\mathbf{H} \\ -2\mathbf{H} & \mathbf{H}^2 + \mathbf{U} \end{bmatrix} \mathbf{Y}_C \right\} \begin{bmatrix} \mathbf{V}_k \\ \mathbf{V}_m \end{bmatrix} \tag{1}$$

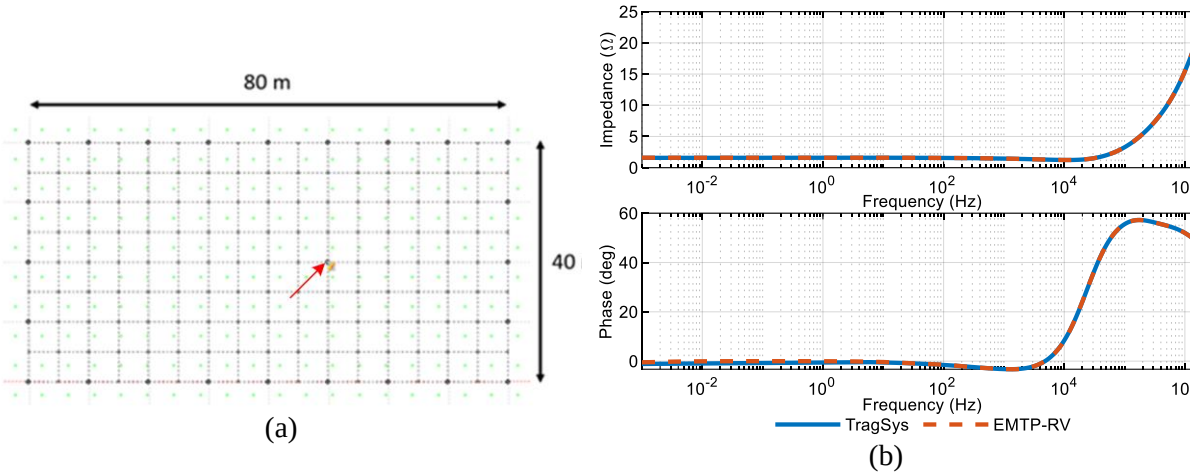

Fig. 3. (a) Substation's grounding grid. (b) Grounding system response.

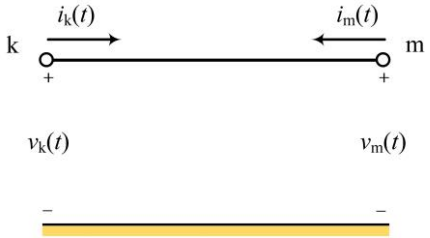

Fig. 4. Transmission line/cable segment.

where **U** is the identity matrix and **H** and $\mathbf{Y}_c$ correspond to the propagation function and characteristic admittance matrices, defined as:

$$\mathbf{H}(\omega) = e^{-\Gamma(\omega)l}; \Gamma(\omega) = \sqrt{\mathbf{YZ}}; \mathbf{Y}_C = \sqrt{\frac{\boldsymbol{Y}}{\mathbf{Z}}} \tag{2}$$

where **Z** and **Y** are the p.u. length series impedance and shunt admittance matrices, respectively.
The line/cable models, similar to other frequency-dependent responses, are implemented in the EMT-type programs using the vector fitting technique. In this regard, the propagation functions **H** and the characteristic admittances $\mathbf{Y}_c$ are approximated by rational functions as:

$$\mathbf{Y}_c \approx \boldsymbol{k}_0 + \sum_{n=1}^{N_{pY}} \frac{\boldsymbol{k}_n}{s - a_n} \tag{3}$$

$$\mathbf{H} \approx \sum_{j=1}^{N_{mod}} \left(\sum_{i=1}^{N_{pH}} \frac{\bar{\boldsymbol{c}}_{\boldsymbol{ij}}}{s - \bar{a}_i} \right) e^{-s\tau_j} \tag{4}$$

where N_{pY} and N_{pH} denote the number of poles while $\boldsymbol{k}_n$ and $\bar{\boldsymbol{c}}_{\boldsymbol{ij}}$ denote the matrices of residues corresponding to $\mathbf{Y}_c$ and **H**. It is worth noting that τ_j is the inherent time delay associated with each of the total N_{mod} propagation modes.

4. TRANSIENT SIMULATION

This section adopts a fictitious setup for studying transformer resonances during transients. In this regard, a single-phase transformer model is developed, with the details shown in Table II. As previously discussed, the vector fitting algorithm is applied to the transformer's admittance matrix. The resulting constants are then implemented into EMT-based software.

Table II. Details of the fictitious transformer.

Number of HV Disks	22
Number of turns per HV disk	40
HV Conductor dimensions	1.8 mm × 8 mm
HV Insulated conductor dimensions	3.11 mm × 9.31 mm
HV inner diameter	750 mm
HV outer diameter	1001 mm
HV Nominal voltage	115 kV
Number of LV turns	50
LV Conductor dimensions	5 mm × 20 mm
LV Insulated conductor dimensions	6 mm × 21 mm
LV inner diameter	600 mm
LV outer diameter	720 mm
LV Nominal voltage	3.45 kV
Turn ratio	0.03

The transformer is connected to a cable of 442.6 m in length which is solidly bonded, with a core diameter of 30 mm, and a total diameter of 55 mm. This cable has a characteristic impedance of 103 Ω and a propagation delay of 2.235 μs. It is important to mention that cable resonance frequencies depend on the length of the cable as well as its per-length capacitance and inductance. Equation (5) represents the fundamental resonance frequency of the cable, f_{res}, as a function of cable length, l, and wave propagation speed in cable, v, [7]:

$$f_{res} = \frac{v}{4l} \tag{5}$$

The cable-transformer compound is connected to the network through a circuit breaker (CB), as demonstrated in Fig. 5. In this study, prestriking transients due to transformer energization are analysed. To such an aim, the CB is modelled considering the gap withstand characteristic corresponding to the distance between its contacts and the high-frequency current chopping according to the following equations [26]:

$$U_B = A(t - t_0) \tag{6}$$

$$\frac{di}{dt} = B \tag{7}$$

where the contact withstand voltage of the CB is denoted by U_B, and its high-frequency current chopping capability is characterized by the critical current derivative di/dt. The contact closing instant is t_0, and the gap withstand characteristic corresponding to the decrease of contact distance is considered by A = −0.1 kV/μs. The critical current derivative for high-frequency current chopping is considered to be constant with B = 350 A/μs [24].

In the following, the transformer energization prestriking transients are analysed in two conditions: with and without cable.

A. Transformer energization transients without cable

Fig. 6 shows the terminal impedance of the HV winding of the transformer with the LV side open, as well as its secondary-to-primary voltage ratio. As can be seen in Fig. 6, the transformer has a major resonance at around 111.5 kHz. Therefore, this resonance frequency can be expected to be excited upon transients. Fig. 6(b) shows the transformer's ratio as a division of the voltage at the LV winding to the voltage at the HV winding terminals over the frequency spectrum. Notably, while the nominal ratio of

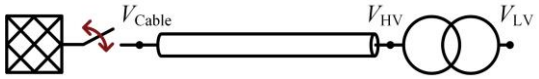

Fig. 5. Single-line diagram of the test system.

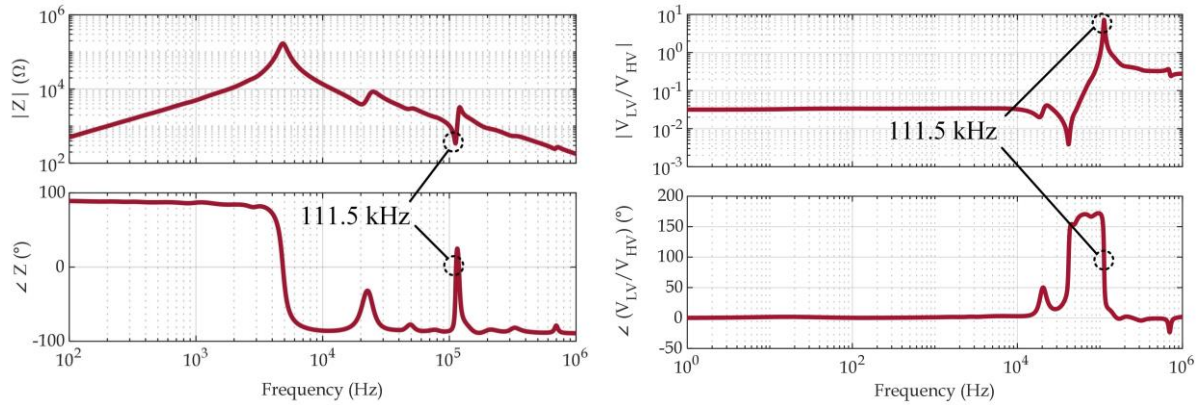

(a) (b)

Fig. 6. Frequency response of test transformer: (a) HV terminal impedance, (b) Voltage ratio.

the transformer around the nominal frequency of 50 Hz has a relatively low value, it rises sharply around the resonance frequency. It is also observed that the impedance phase angle at the resonance frequency is zero, and the voltage components at the resonance frequency are perpendicular, thus characterizing a phase difference of ±90° in the voltage transfer ratio.

The transformer is energized by a sinusoidal source at the line-to-line RMS voltage of 115 kV. In this regard, the contact closing time is set at the peak of the excitation voltage. The voltages upon transformer energization are demonstrated in Fig. 7. The voltage across the CB is shown in Fig. 7(a), where dashed lines represent the contact withstand voltage. The voltage at the transformer's HV and LV terminals have been illustrated in Figs. 7(b) and 7(c), respectively. CB prestrikes shown in Fig. 7(a) have imposed steep transients on the transformer's HV terminal, represented in Fig. 7(b). These transients have, in return, excited high-frequency resonance modes of the transformer, causing the oscillating overvoltages observed at the LV terminal, as shown in Fig. 7(c). As expected from the transformer's coupling ratio, the high-frequency transients have been transferred from the transformer's HV side to its LV side with high amplitudes.

B. Transformer energization transients with cable

In this subsection, transformer energization transients have been analysed considering the presence of

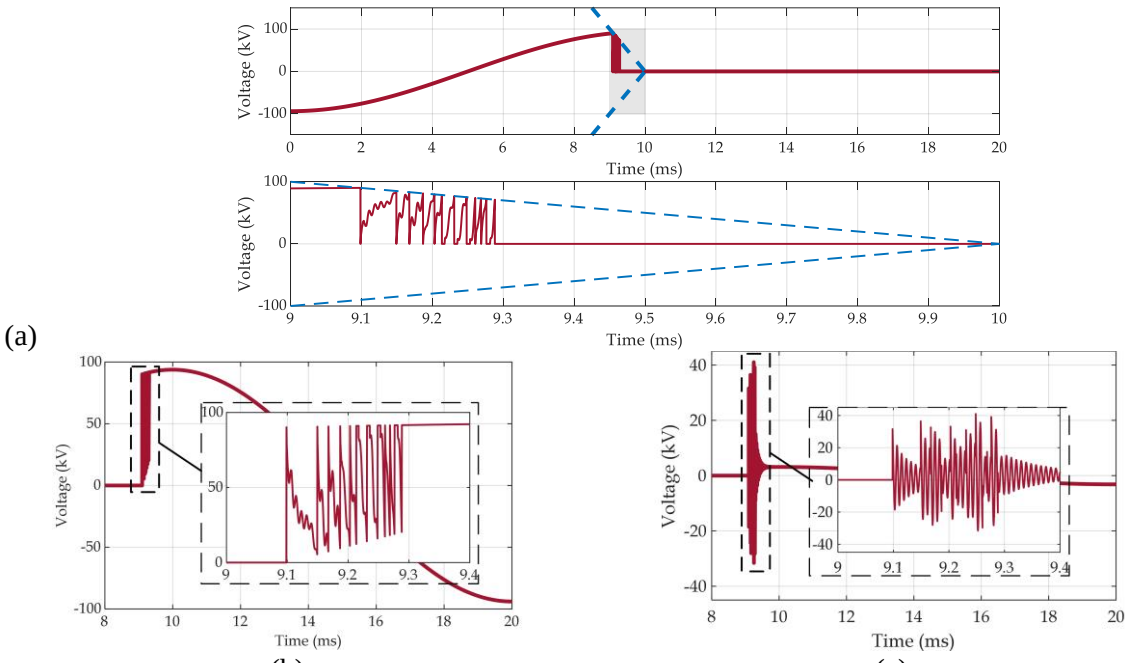

(a) (b) (c)

Fig. 7. Energization transients for transformer without cable: (a) Voltage across CB, (b) Voltage on transformer HV terminal, (c) Voltage on transformer LV terminal.

the introduced cable between the switchgear and the transformer's HV terminal. The harmonic impedance of the transformer at the HV terminal, the short circuit impedance of the cable, and the total impedance of the cable–transformer compound have been demonstrated in Fig. 8(a). As can be seen, the cable's first resonance frequency coincides with the transformer's major resonance frequency at 111.5 kHz. In this condition, due to the mutual interactions between the cable and the transformer, the resonance point is split into two resonance frequencies of 103.3 kHz and 115.9 kHz. Fig. 8(b) illustrates the voltage ratio between the transformer's LV terminal and the cable. As shown in Fig. 8(b), the presence of the cable has led to a drastic increase in voltage ratio to the secondary side of the transformer. It is worth mentioning that the voltage components at the two resonance frequencies of 103.3 kHz and 115.9 kHz are perpendicular, corresponding to phase shifts of +90° and -90°, as shown in Fig. 8(b).
Similar to the previous subsection, the CB energizes the cable–transformer compound with a contact closing time of 10 ms. Fig. 9 illustrates the transients upon CB closing, considering the energization of the transformer through the cable. Fig. 9(a) shows multiple prestrikes as the withstand voltage between CB contacts decays. Compared to the case without the cable, the observed prestrikes characterize higher variations and are spread along the total interval until the CB is fully closed. This condition indicates the recurrence of high transient recovery voltages (TRVs) upon arc extinguishment in the CB. The presence of the cable has led to excessive voltage build-up on the transformer HV terminal, as demonstrated in Fig. 9(b). These increased voltages, on the one hand, and the high voltage ratio around the resonance frequency, on the other hand, have led to severe resonating overvoltages on the transformer's LV terminal up to around 170 kV, as shown in Fig. 9(c). It is worth noting that the beating voltage waveform in Fig. 9(c) is formed due to the simultaneous excitation of two nearby resonance frequencies at 103.3 kHz and 115.9 kHz.

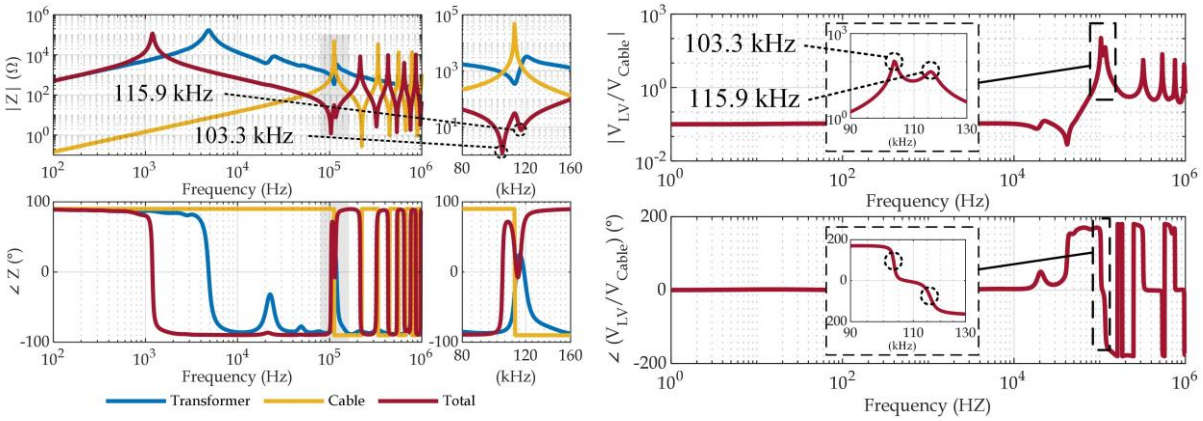

(a) (b)

Fig. 8. Frequency response of test transformer with cable connected to HV terminal: (a) Impedance responses, (b) Voltage ratio.

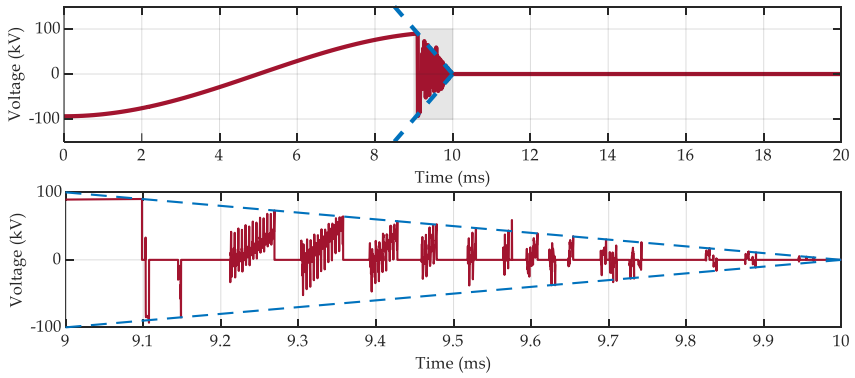

(a)

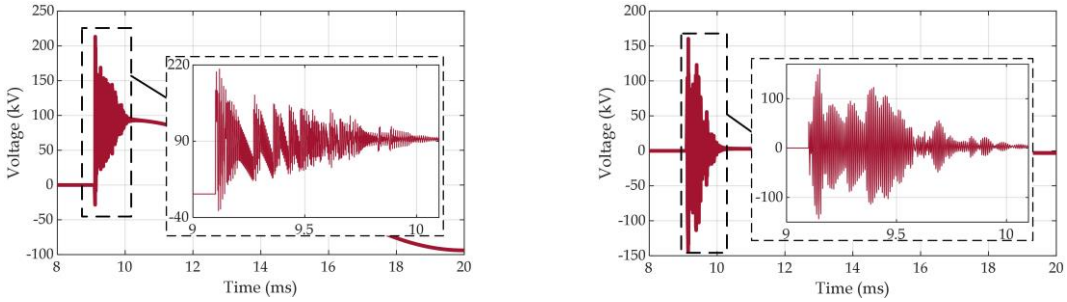

(b) (c)

Fig. 9 Energization transients for transformer with cable: (a) Voltage across CB, (b) Voltage on transformer HV terminal, (c) Voltage on transformer LV terminal.

5. PROTECTION METHOD

This section discusses the main features and effects of the series-type protection device consisting of a ring core and a resistive suppressor as a secondary circuit of the ring core. The existing well-known shunt protection devices, such as surge capacitors, RC snubbers, and ZORCs, are indeed very practical for suppressing transient signals at low and medium-voltage levels. However, these devices typically exhibit high reactive power consumption, which makes them less suitable for application in high-voltage power transmission systems. Unlike the conventional shunt protection devices, this proposed solution consumes almost negligible reactive power during the system's normal operation. This is an important advantage, as it allows the protection device to be effectively deployed in high-voltage transmission networks without significantly impacting the overall reactive power balance of the system. The principle of the series-type protection methods against voltage transient signals is based on reducing the magnitude of specific frequency content of the transient waveform as well as decreasing the voltage variation rate. Fig. 10 illustrates the configuration of the proposed series protection device integrated with a transformer and cable. This figure shows that the protection device (blue box) is connected in series between the transformer and cable, where its voltage drop $v_p(t)$ decreases the transient voltage of the transformer $v_{tr}(t)$. The operation principle is defined by (8):

$$v_{tr}(t) = v_n(t) - v_p(t) \tag{8}$$

Here, $v_n(t)$ is a transient voltage at node "n". Fig. 11 depicts the series protection device structure in configuration with a cable and transformer.

The design procedure of the series protection device is prepared by considering the critical resonance point of the transformer and features of the voltage transient signal. In the first stage, the required

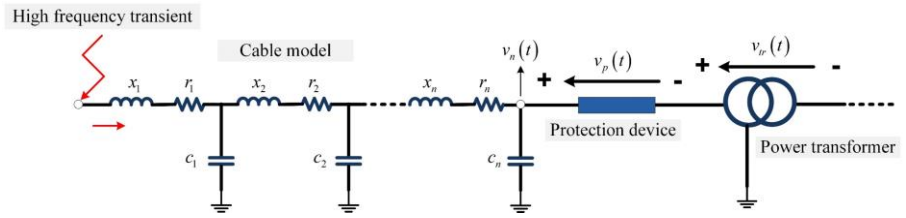

Fig. 10. Protection device configuration with the transformer and cable.

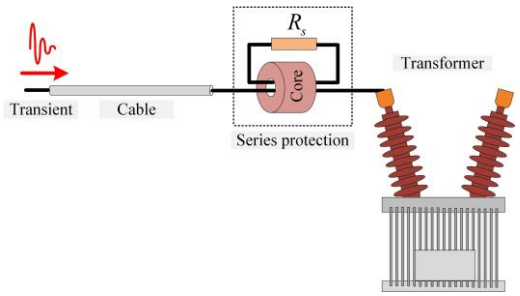

Fig. 11. Protection device configuration with the transformer and cable.

impedance imposed by the series protection is determined by obtaining the impedance of the transformer in resonance conditions. In the subsequent stage, the protection device core size is computed to ensure acceptable impedance, effectively suppressing the magnitude of transient signals while operating out of the saturation region. In the final phase of the design process, the selection of the resistor on the secondary side of the ring core is paramount. This decision is based on evaluating both the assumed magnitude of the transient signal and the power loss in the resistor. If the initially calculated power loss exceeds the resistor's capacity, its specification should be recalculated to bring it within an acceptable threshold of power loss. Regarding the energy dissipation in the resistor, the peak current can reach several kiloamperes during transient conditions. However, considering a typical transient signal duration of 50 microseconds, the maximum energy dissipation in the resistor would not be significant. The level of energy dissipation is not excessively large and can be effectively managed through regular geometric design of the resistor and the use of a heat sink. Fig. 12 shows the design procedure of series protection of the transformer against transient voltage in a flowchart diagram.

Regarding v_n (the transient voltage at the terminal of the protection device) in Fig. 10, this voltage can be divided into the voltage drop over the protection device and transformer during the transient phenomenon. Indeed, at the resonance frequency of the transformer, which causes transformer overvoltage, the transformer's relatively low impedance and the choke's high impedance result in a drastic decrease of the transient signal magnitude at the transformer resonance frequency. Accordingly, the vital conditional equations to safeguard the transformer are presented in (9)-(12).

$$V_{tr} \leq V_{sg} \tag{9}$$

$$V_{tr} = \frac{V_n . Z_{tr}}{Z_{tr} + Z_p} \tag{10}$$

$$\frac{V_n . Z_{tr}}{Z_{tr} + Z_p} \leq V_{sg} \tag{11}$$

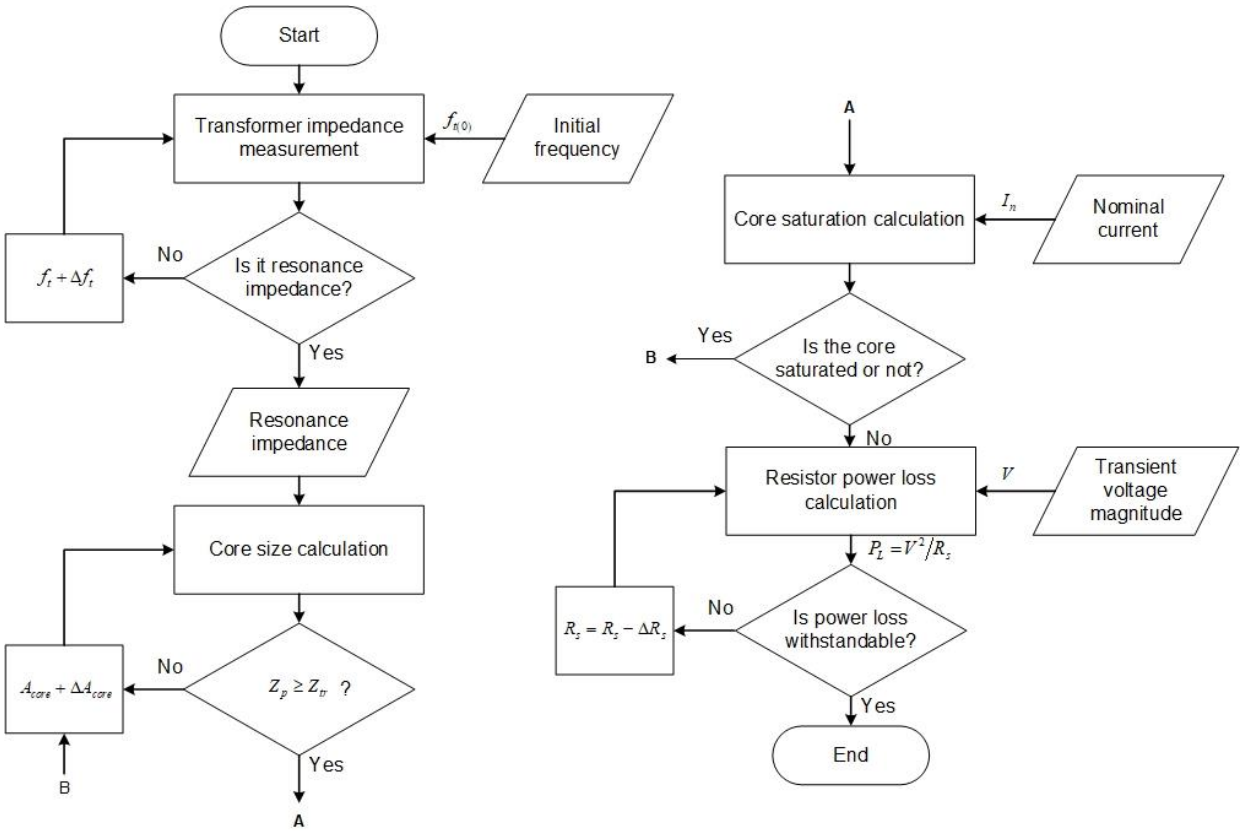

Fig. 12. Series protection design procedure.

$$\left(\frac{V_n.Z_{tr}}{V_{sg}}\right) - Z_{tr} \leq Z_p \tag{12}$$

Here, V_{tr}, V_n, and V_{sg} are the transformer's voltage, node "n" voltage, and the safeguarding voltage level, respectively. In (9), it is assumed that the voltage of the transformer must be equal to or less than a safeguarding voltage. Also, Z_{tr} and Z_p are the transformer and protection device impedance. Considering that the studied frequency is a resonance frequency of the transformer f_r, the value of the resistance R_s and inductance of the protection device L_s can be computed according to the equation (13):

$$\left(\frac{V_{n(fr)}.Z_{tr(fr)}}{V_{sg}}\right) - Z_{tr(fr)} \leq \frac{R_s.j2\pi f_r L_p}{R_s + j2\pi f_r L_p} \tag{13}$$

Fig. 13 presents the impedance response of an example series protection device, demonstrating that its impedance is just a few milliohms at the power system frequency. As seen in the illustration, the impedance of series protection changes linearly with frequency. The choke operates in a frequency domain between 70 kHz and 1 MHz, where the imposed impedance value varies between 100 Ω and 1.5 kΩ. It is worth noting that the protection device appears to be effective, even in the face of modeling uncertainties. These uncertainties could lead to resonance shifts, deviating from reality. However, the characteristic impedance of the device offers the necessary flexibility to manage these challenges, facilitating more effective parameter selection.

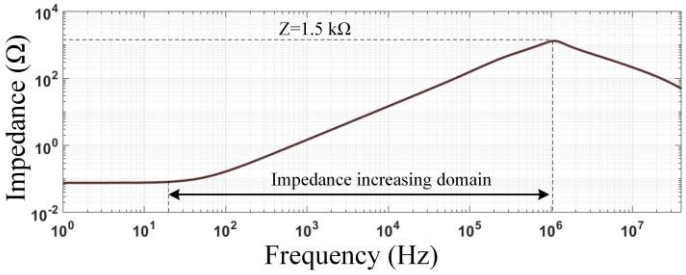

Fig. 13. An instance frequency response of series protection device.

Through the integration of the series protection device with the cable and the transformer model, focus is put on the system's impedance around the resonance point, as illustrated in Fig. 14. The red curve in the figure represents the system impedance near the resonance point, showing a significant decline of only several ohms. This notable reduction in impedance is mainly attributed to overvoltage in the transformer.

Connecting the series protection to the transformer compensates the system impedance by imposing the impedance of the series protection device, effectively suppressing overvoltage. The blue graph in the figure shows a significant improvement in the system's response after applying the protection device. As it is observable, dangerous conditions around the resonance frequencies are well alleviated, especially around the targeted frequency of matched cable and transformer resonances. The increase in impedance at these resonance points provides protection for the transformer against overvoltage, ensuring its safeguarding. Furthermore, this increase in impedance around resonance points can suppress other resonance around the main resonance frequency and also ensure suppression of shifted resonance frequency.

In order to evaluate the performance of the protection device in time domain, similar to previous sections, EMT simulations of transformer energization have been carried out, with the protection device present in the circuit. Simulation results have been represented in Fig. 15. Comparing the results demonstrated in Fig. 9 (without protection) and Fig. 15 (with protection), one can observe the excellent performance of the protection device in mitigating the severe resonating overvoltages excited in the cable-transformer system. It is notable that the terminal voltages have been alleviated from

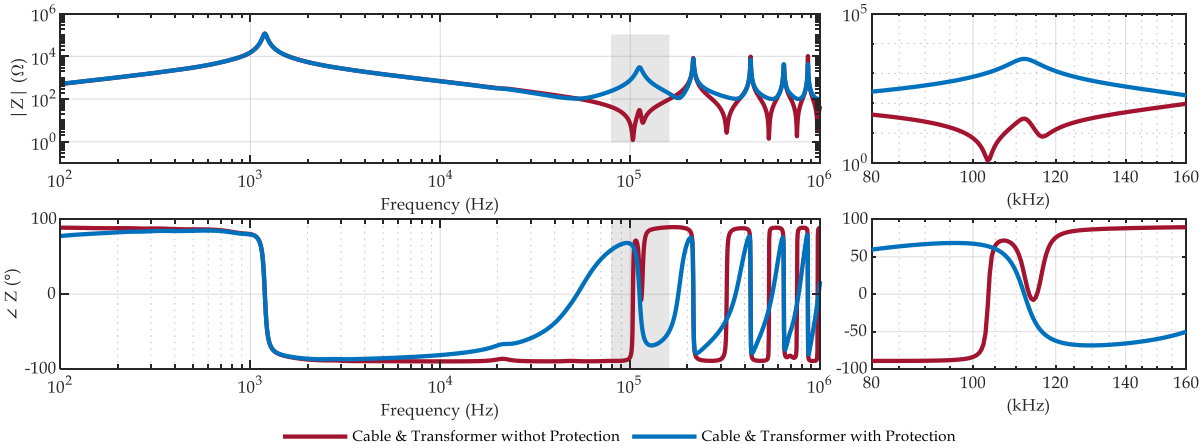

Fig. 14. System impedance response with and without series protection device.

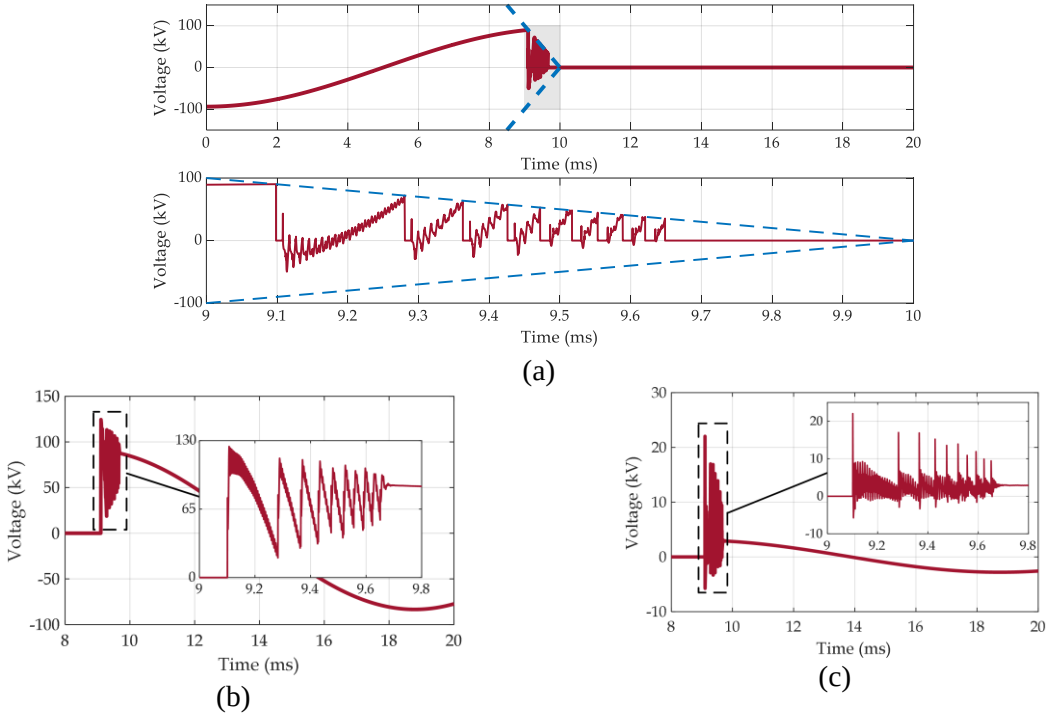

Fig. 15. Energization transients for cable and transformer after applying protection: (a) Voltage across CB, (b) Voltage on transformer HV terminal, (c) Voltage on transformer LV terminal.

around 215 kV to around 125 kV at the HV side and from around 160 kV to around 22 kV at the LV side.

CONCLUSION

The paper presents physics-based analytical models and analysis approaches to study transformer vulnerabilities and develop a protection solution for emerging grid transient threats. A transformer winding model has been developed to calculate voltage distribution in the windings and determine its resonant frequencies. The model has been validated through comparison with experimental measurements. Examining transformer energization transients with and without a connected cable underscores the critical impact of resonances and coupling ratios on system behaviors. This analysis shows the risk for resonating overvoltages and transient recovery voltages under different system configurations. Utilizing the data obtained through simulations, a protection device against transients has been developed. This scheme aims to provide an impedance that dominates the transformer's

impedance at resonance frequencies, suppressing any overvoltages that may occur. The series connection avoids issues like high-frequency grounding impedances in shunt mitigation solutions. The protection device's design procedure is presented, and its impedance response demonstrates the effectiveness of the protection device against the critical resonance point of the transformer by increasing the system impedance around the resonance points.

ACKNOWLEDGMENT

This research work has been financially supported by the Dutch Scientific Council NWO-TTW in collaboration with TSO TenneT, DSO Alliander/Qirion, Royal Smit Transformers, and TSO National Grid, UK, under the project “Protection of Future Power System Components (PRoteuS)”, no. 18699.

BIBLIOGRAPHY

[1] A. da CO Rocha, A. Holdyk, B. Gustavsen, B. Jaarsveld, A. Portillo, and M. Popov, "Electrical transient interaction between transformers and the power system - part I. Expertise," Joint Working Group A2/C4.39: Cigré, 2014.

[2] M. Popov, L. Grcev, H. K. Hoidalen, B. Gustavsen, and V. Terzija, "Investigation of the overvoltage and fast transient phenomena on transformer terminals by taking into account the grounding effects," IEEE Transactions on Industry Applications, vol. 51, no. 6, pp. 5218-5227, 2015.

[3] A. Cancino, R. Ocón, G. Enríquez, and R. Malewski, "In service failure of 230 kv transformers due to steep-front lightning over voltages at mexican west coast," in CIGRE session, 2006.

[4] M. Popov, R. P. P. Smeets, L. van der Sluis, H. de Herdt, and J. Declercq, "Experimental and theoretical analysis of vacuum circuit breaker prestrike effect on a transformer," IEEE transactions on power delivery, vol. 24, no. 3, pp. 1266-1274, 2009.

[5] G. C. Paap, A. Alkema, and L. Van der Sluis, "Overvoltages in power transformers caused by no-load switching," IEEE transactions on power delivery, vol. 10, no. 1, pp. 301-307, 1995.

[6] B. Gustavsen, "Study of transformer resonant overvoltages caused by cable-transformer high-frequency interaction," IEEE Transactions on Power Delivery, vol. 25, no. 2, pp. 770-779, 2010.

[7] A. Holdyk and B. Gustavsen, "External and internal overvoltages in a 100 MVA transformer during high-frequency transients," in Proceedings of the International Conference on Power System Transmission (IPST), Cavtat, Croatia, 2015, pp. 15-18.

[8] P. Akiki, A. Xémard, C. Trouilloud, and J.-L. Chanelière, "Study of high frequency transient overvoltage caused by cable-transformer quarter-wave resonance," Electric Power Systems Research, vol. 197, p. 107295, 2021.

[9] L. Zhou, L. Huang, R. Wei, and D. Wang, "A novel lightning overvoltage protection scheme using magnetic rings for transmission line systems," IEEE Transactions on Industrial Electronics, 2023.

[10] S. M. Korobeynikov, S. I. Krivosheev, S. G. Magazinov, V. A. Loman, and N. Ya, "Suppression of incoming high-frequency overvoltage in transformer coils," IEEE Transactions on Power Delivery, vol. 36, no. 5, pp. 2988-2994, 2020.

[11] D. Smugała, W. Piasecki, M. Ostrogorska, M. Florkowski, M. Fulczyk, and P. Kłys, "Distribution transformers protection against high frequency switching transients," PRZEGLĄD ELEKTROTECHNICZNY (Electrical Review), ISSN, pp. 0033-2097, 2012.

[12] D. Smugała, W. Piasecki, M. Ostrogórska, M. Florkowski, M. Fulczyk, and O. Granhaug, "New approach to protecting transformers against high frequency transients–wind turbine case study," Prz. Elektrotech, vol. 89, pp. 186-190, 2013.

[13] F. Nasirpour, A. Heidary, M. G. Niasar, A. Lekić, and M. Popov, "High-frequency transformer winding model with adequate protection," Electric Power Systems Research, vol. 223, p. 109637, 2023.

[14] A. Heidary, M. G. Niasar, M. Popov, and A. Lekić, "Transformer resonance: reasons, modeling approaches, solutions," IEEE Access, 2023.

[15] B. Gustavsen, et al., "High-frequency transformer and reactor models for network studies, part a: white-box models," Conseil International des Grands Réseaux Électriques (CIGRE) TB 900, pp. 1-203, 2023.

[16] S. H. Hosseini, M. Vakilian, and G. B. Gharehpetian, "Comparison of transformer detailed models for fast and very fast transient studies," IEEE transactions on power delivery, vol. 23, no. 2, pp. 733-741, 2008.

[17] E. Rahimpour, J. Christian, K. Feser, and H. Mohseni, "Transfer function method to diagnose axial displacement and radial deformation of transformer windings," IEEE Transactions on power delivery, vol. 18, no. 2, pp. 493-505, 2003.

[18] L. Grcev and F. Dawalibi, "An electromagnetic model for transients in grounding systems," IEEE Transactions on power Delivery, vol. 5, no. 4, pp. 1773-1781, 1990.

[19] L. D. Grcev, "Computer analysis of transient voltages in large grounding systems," IEEE Transactions on power delivery, vol. 11, no. 2, pp. 815-823, 1996.

[20] "TRAGSYS-Software for High Frequency and Transient Analysis of Grounding Systems. [Online]." http://www.tragsys.com.

[21] B. Gustavsen, and A. Semlyen, "Rational approximation of frequency domain responses by vector fitting," IEEE Transactions on power delivery, vol. 14, no. 3, pp. 1052-1061, 1999.

[22] B. Gustavsen, "Improving the pole relocating properties of vector fitting," IEEE Transactions on Power Delivery, vol. 21, no. 3, pp. 1587-1592, 2006.

[23] D. Deschrijver, M. Mrozowski, T. Dhaene, and D. De Zutter, "Macromodeling of multiport systems using a fast implementation of the vector fitting method," IEEE Microwave and wireless components letters, vol. 18, no. 6, pp. 383-385, 2008.

[24] L. Grcev and M. Popov, "On high-frequency circuit equivalents of a vertical ground rod," IEEE Transactions on power delivery, vol. 20, no. 2, pp. 1598-1603, 2005.

[25] J. A. Martinez-Velasco, Power system transients: parameter determination. CRC press, 2017.

[26] S. Ghasemi, M. Allahbakhshi, B. Behdani, M. Tajdinian, and M. Popov, "Probabilistic analysis of switching transients due to vacuum circuit breaker operation on wind turbine step-up transformers," Electric Power Systems Research, vol. 182, p. 106204, 2020.